Dandao Xuebao/Journal of Ballistics
ISSN: 1004-499X
Vol. 37 No. 1 (2025)

Adsorption of Selected NSAIDs, Diclofenac Potassium, Piroxicam-beta-cyclodextrin and Paracetamol onto Activated Carbon/ Iron Oxide Nanocomposite from Wastewater: Experimental and DFT Approach

Saeed Ullah Jan[1,2*], Waqas Ahmad[2], Abdur Rahman[2] Anjum Begum[2], Abuzar khan[2], Jabir Khan[3], Hajira Bibi[2], Imtiaz Ahmad[2], Bushra Bostan[1], and Muhammad Zahid Khan[3]

[1] Department of Chemistry, Chakdara Lower Dir, 18800, University of Malakand, Pakistan
[2] Department of Chemistry, Government post graduate college Timergara, Lower Dir, 18300, Pakistan
[3] Department of Physics, Gomal University Dera Ismail Khan, 29111, KPK, Pakistan
* saeedsimaab@gmail.com

Abstract: The adsorption of NSAIDs on activated carbon/ Fe_2O_3 nanocomposite prepared by simple coprecipitation method was investigated by batch technique. The composition of the composite was investigated by different characterization techniques, including XRD, SEM, FTIR and TGA. Subsequently, the composite was utilized to remove painkillers, namely diclofenac potassium, piroxicam-beta-cyclodextrin and paracetamol from aqueous solutions. Numerous factors affecting the adsorption process were investigated including contact time, pH, adsorbate concentration, temperature, and adsorbent dosage were systematically optimized. The optimal adsorption for piroxicam-beta-cyclodextrin (94.2%), diclofenac potassium (96.2%), and paracetamol (94.9%) were achieved at pH 2, 4 and 7 respectively. Adsorption data were analyzed, by using different adsorption isotherms. Diclofenac potassium and paracetamol obeyed more closely the Freundlich isotherm model, as compared to other models, while piroxicam-beta-cyclodextrin exhibited conformity with the Temkin isotherm model across the entire concentration spectrum. The kinetic analysis indicates that the adsorption of all three adsorbates obey pseudo-second-order kinetics. The thermodynamic analysis yielded the following parameters: ΔH = -63.04 kJ/mol, ΔS = -167.79 J mol^{-1} K^{-1} for diclofenac potassium, ΔH = -10.89 kJ/mol, ΔS = -35.11 J mol^{-1} K^{-1} for piroxicam-beta-cyclodextrin and ΔH = -68.83 kJ $mol^{-1,}$ ΔS = -217.22 for paracetamol. These findings suggest that the adsorption process is not only spontaneous but also exothermic, resulting in the release of heat. The DFT calculations unveiled significant interactions between the active sites of all painkillers and the AC/Fe_2O_3 composite, as confirmed by their negative binding energies.

Keywords: Pharmaceutical agent; adsorption; banana peel-derived activated carbon /Fe_2O_3 nanocomposite; DFT

1. Introduction

The contaminants released by pharmaceutical industries, have harmful effects on both the environment and human health, when accumulate in the surface of water through various pathways, such as improper disposal of unused medicine, aquaculture treatment, and wastewater treatment [1]. Approximately, 2 million metric tons of pollutants are released into fresh water daily [2]. These pollutants, originated from sources like pharmaceutical industries, hospital effluents and treatment plant waste etc. has become one of the top environmental concerns. When purification systems can't get rid of them, these pollutants make their way into lakes, rivers, and even fresh water networks [3, 4]. According to the UN Annual Report, about 1500 km^3 of wastewater is produced each year, which is roughly six times the volume of current river water [5]. Pharmaceuticals are chemical compounds developed to cure human diseases [6]. These pharmaceuticals fall into the seven major categories, including analgesics, antibiotics, antiepileptics, stimulants, opioids, dopamine agents, and antiseptics, contributing to a pressing concern, because of their dual influence on both the environment and human health. [1, 7]. The occurrence of pharmaceuticals in municipal wastewater and effluents is the main source of its occurrence in drinking water. In this vein, non-steroidal anti-inflammatory drugs (NSAIDs) are among the most commonly detected pharmaceuticals in wastewater since they are abundantly used as analgesics, antipyretics, and anti-inflammatories. Thus, they have

been recognized as emerging contaminants with long-lasting harmful impacts on the living components in the environmental system as well as on human health. Therefore, there is a continuing demand for efficient, green, and sustainable techniques for the removal of NSAIDs from wastewater. [8, 9]. Due to their availability as over-the-counter drugs and their comfort of purchase from the market without a specific prescription, NSAIDs are the type of drugs, which are extensively utilized [8]. The paracetamol, acetylsalicylic acid, diclofenac, ibuprofen and naproxen are among the more popular drugs in this class. The white crystalline substance, paracetamol, (4-hydroxyacetanilide) is used for the treatment of negligeable pain and to reduce body temperature in cases of fever [8, 10]. Additionally, many pharmaceuticals in healthcare contain paracetamol as a primary ingredient and comes in various formulation and are generally regarded as safe, with exception of excessive dose [8, 11]. In the recent years, advanced analytical methods have raised awareness of the existence of drugs, pharmaceuticals, pesticides, food, personal care products, additives and various contaminant residues in the water [3]. Environmental problems have reached a critical point, necessitating immediate action to safeguard public health by decrease pollutants [12]. *Available remediation methods for achieving this protection encompass a wide range of techniques, including aerobic/anaerobic and biological digestion* [13]*, germicidal UV treatment, hydrodynamic cavitation, chemical processes like ozonation, photocatalysis, Fenton, photo-Fenton, electrochemical methods, electro-Fenton, electrocatalysis,* [13, 14]*, oxidative processes, as well as physical procedures such as adsorption, coagulation, sedimentation, flocculation, magnetic separation and membrane* [15]. Adsorption stands out as the preferred method for removing a broad range of pharmaceuticals pollutants from water-based solutions, because of its simplicity, convenience of use, and wide spectrum of adsorbents.[16]. Numerous studies have investigated pharmaceutical compound adsorption onto various adsorbents, including agricultural activated carbon from agricultural sources, metal oxide nanoparticles, polymer composites, and metal hydroxides, among other things, untreated agricultural wastes [17]. Choosing a cost-effective adsorbent with ample adsorption sites and effective intermolecular interactions with pharmaceutical waste in wastewater is of utmost importance. Activated carbons (Ac), isolated biopolymers, agricultural wastes and their composites are suitable series of adsorbents, meeting these criteria. These materials are deemed highly promising adsorbents because of their cost-effectiveness, abundance, and versatile surface functional groups that readily interact with pharmaceutical molecules. These adsorbents have a track record of effectively removing synthetic dyes [18, 19]. These intricate dyes have interacting functional groups and an aromatic ring structure, which are comparable to those of common pharmaceuticals, making it possible to use the same techniques. The adsorption of STM (streptomycin), IBU (ibuprofen), and RIF (rifampicin) at high capacities onto various adsorbents, such as sodium thiosulphate-modified thalia dealbata activated carbon [20], activated bamboo waste and chitosan/Fe_3O_4, according to reports [21, 22], pectin and Chitosan, derived from agricultural wastes and food, are shown superior adsorbents for removing fluoride ions and synthetic dyes [18], [23]. Building on this understanding, our study explores Fe_2O_3 grafted graphene oxide as an adsorbent for common NSAIDs (non-steroidal anti-inflammatory drugs). The computational methods employed in this research encompass a range of theories, including Post Hartree Fock (PHF), MP2, and Hartree Fock (HF) [24, 25]. However, Density Functional Theory (DFT) has garnered significant attention recently due to its correctness and practicality [26]. Introduced in 1964 by Pierre Honenberg and Walter Kohn, DFT utilizes electronic probability density to compute ground state energy and electronic characteristics [27, 28]. The Kohn-Sham modification played a pivotal role in shaping DFT, leading to the development of the Density Functional Version (DFV) comprising distinct equations for energy determination related to Kohn-Sham orbitals [29, 30]. DFT is gaining prominence across various systematic domins including chemistry, materials science, biology and physics and can be represented as E = T + U + V + W, where T stands for Kohn-Sham orbital energy, U for Hartree energy, V for electron-nucleus attraction, and W for exchange correlation functional energy [31, 32]. Moreover, DFT serves as the fundamental method for modelling atomic orbitals and molecular structures, utilizing functions like Slater and functions, with Gaussian applications extending to material research and pharmaceutical synthesis via tools like DMole3 [33, 34].

This motivated us to design a greener method for the synthesis of a nanocomposite of iron oxides ($Fe2O_3$) and activated carbon to be applied as an adsorbent for NSAIDs. Activated carbon is a two-dimensional nanostructure composed of stacks of carbon sheets that appear as platelets and feature a large surface area that offers a great adsorption capacity and a typical host platform to generate diverse nanocomposites. The impact of the entire process on the environment and operator safety was also explored.

2. Reagents

The chemicals, including sodium hydroxide (NaOH), zinc chloride ($ZnCl_2$), ferrous sulphate ($FeSO_4$) and ferric chloride ($FeCl_3$) were of analytical grade, sourced from Sigma-Aldrich, and used without further purification.

2.1. Apparatus

A pH meter with a pH range of 1 to 10 was used in this study, along with other instruments i.e. (Perkinelmer, L1600300 Spectrum Two) FTIR spectrometer, UV-VIS. spectrophotometer (Labomed, Inc. UVD-2960), (Model-75) wrist action shaker, scanning electron microscope (SEM, JSM-5910 model), X-ray diffraction (XRD, JDX-3532 model), and thermogravimetric analyser (Pyris Diamond Series TG/DTA and TGA).

2.2. Adsorbent material

2.2.1. The method of making activated carbon

Utilizing banana peels, activated carbon was made [35, 36]. The peels came from a local market in Timergara City, Pakistan. The banana peel was washed with distilled water to remove the remaining dust materials. The size of the peel was reduced from 1 to 2 cm to accelerate the drying process. After all the dripping water was sun-dried, the peel was placed in an oven for 24 h at 105 °C to remove the moisture content. The dried peel was powdered using an attrition mill. The powdered banana peel was sieved (IC-205/EV) and the particle size below 125 μm was retained. It was then weighed and packed in an air-tight plastic bag. Then the sample was subjected to 350 °C at a rate of 10 °C/min for 3 h in a furnace under an N2 environment, based on the method adopted by Zamora-Ledezma et al. (2021). After being cooled and size reduced to 125 μm, the sample was further activated chemically at different operating conditions. The acid activation with variation in acid concentration, temperature and activation time. Acid activation is one of the most common chemical treatments and has been used to increase the specific surface area and the number of acidic centres, modify the surface functional group and obtain solids with high porosity [37].

2.3. The composite of activated carbon and iron oxide (AC/Fe_2O_3)

The synthesis of the AC/Fe_2O_3 composite involved the co-precipitation method. [38]. A mixture of freshly prepared ferrous sulphate (10 ml) and iron chloride (10 ml) solutions were stirred for 30 minutes at 60°C. Then, 2 g activated carbon was added to these solutions, and it was stirred for an additional 40 minutes at 30°C. Subsequently, 2M NaOH solution was incrementally (1 ml at time) introduced until the pH reached a range of approximately 10 to 11. After another hour of mixing, the solution was maintained at an ambient room temperature for a period of 24 hours. The collected sample was meticulously rinsed with distilled water, followed by ethanol, and subsequently subjected to drying at 80°C.

2.4. Adsorbates

Three different types of pain relievers served as adsorbates in this investigation, namely paracetamol, Formula: $C_8H_9NO_2$
Boiling point: 420 °C
Density: 1.29 g/cm³
Melting point: 169 °C
IUPAC ID: N-(4-hydroxyphenyl) acetamide, N-(4-hydroxyphenyl) ethanamide, piroxicam-beta-cyclodextrin
Chemical formula: $C_{57}H_{83}N_3O_{39}S$
Melting point: 501 °C
Molar mass: 1134.987 g·mol^{-1}

Solubility in water: 18.5 g/L
IUPAC name: 4-Hydroxy-2-methyl-N-(2-pyridinyl)-2H-1,2-benzothiazine-3-carboxamide 1,1-dioxide

and diclofenac potassium. Chemical formula: $C_{14}H_{10}C_{l2}KNO_2$
Melting point: 302-310°C
Molar mass: 334.237 g·mol−1
IUPAC name: 2-[2-(2,6-dichloroanilino) phenyl] acetic acid.
The chemical structures of these compounds are depicted in (Figures 1a, b, c) corresponding to diclofenac potassium, piroxicam-beta-cyclodextrin and paracetamol individually.

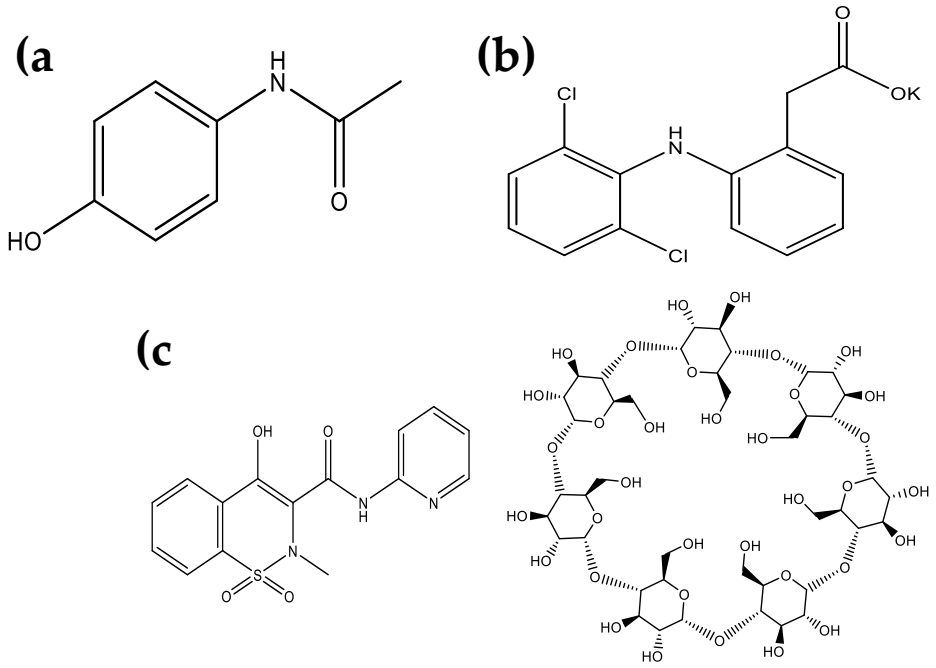

Figure 1. (a) Paracetamol, (b) Diclofenac potassium and (c) Piroxicam-beta-cyclodextrin.

2.5. Experimental Methodologies

2.5.1. Stocks Solution

For each painkiller, a stock solution (500 ppm) was prepared by placing 0.1 g of the respective painkiller in a volumetric flask with a 500 ml capacity, and then topping it up with distilled water to the marked line. These solutions were subsequently employed as needed.

2.5.2. Maximum wavelength determination (λmax)

To determine the maximum wavelength possible (λmax), solutions with varying concentrations of pain relievers were meticulously prepared and subjected to UV-Vis scanning within its range from 200-800 nm using UV-Vis spectrophotometer. The observed maximum wavelengths (λmax) for paracetamol, piroxicam-beta-cyclodextrin, and diclofenac potassium were recorded as 243 nm, 352 nm and 270 nm respectively.

2.5.3. Calibration Curves

Calibration curves were generated by plotting the absorbance against the concentration (ppm) of various adsorbate solutions. Fig. S 1 (a), the calibration curves for paracetamol, diclofenac potassium, and piroxicam-beta-cyclodextrin show the R^2 values of 1 or nearly 1.

2.5.4. pH solutions preparation

Solutions with different pH values, between pH 1 and 10, were carefully prepared for this study. Hydrochloric acid solutions were diluted to produce pH values between 1 and 6, while pH levels of 8 to 10 were attained by diluting sodium hydroxide. All pH solutions were meticulously adjusted and verified using both a pH paper and pH meter.

2.5.5. Adsorption studies

In the batch-mode experiment, a specific amount of the adsorbate and the AC/Fe_2O_3 composite were combined in culture tubes and agitated using a wrist action shaker for a specific duration. After mixing, the specimens were filtered and underwent spectrophotometric examination to assess the adsorbate's concentration. This experimental procedure was conducted in triplicate. The percentage removal (% removal) and the adsorption equilibrium (q_e) of the painkillers were ascertained using the following equations [39].

$$\% \text{ Adsorption} = \left(\frac{C_o - C_e}{C_o}\right) \times 100 \qquad (1)$$

$$qe = C_o - C_e \times \frac{V}{m} \qquad (2)$$

In this context, V represents the volume of the solution in dm^3, Co stands for the initial adsorbate concentration, Ce denotes the equilibrium or final concentration, and 'm' represents the mass of the adsorbent.

2.6. Computational specification

The equilibrium geometries were computed using the Perdew-Burke-Ernzerhof (PBE) correction within the framework of the generalized gradient approximation (GGA) [40]. Van der Waals forces were considered in the calculations using the DFT-D method, following Grimme's approach [41]. For this calculation, the choice of the double numerical polarization (DNP) atomic orbital basis set included a real-space global cutoff radius of 4.6. In the computational process, a Fermi smearing parameter of 0.005 HA was employed [42]. The maximum force, maximum displacement, and maximum energy convergence requirements were established at 1 x 10^{-5} Ha, 0.005, and 0.001 Ha -1 individually. The DMOl3 method was used for all of the DFT calculations. [43].
This is how the adsorption energies (Ead) were determined. [44]:

$$E_{ad} = E_C - (E_S + E_A) \qquad (3)$$

In this case, E_C signifies the overall energy of the complicated system, encompassing the adsorption of painkillers onto composite surfaces. E_S corresponds to the total energy of isolated monomer surfaces, while E_A represents the complete energy of the adsorbate molecules. An evaluation of the charge transfer was performed using Hirshfeld charge density analysis [45].

3. Experimental section

3.1. Characterization

The characterization of the composite involved the use of SEM, XRD and FTIR.

3.1.1. Scanning Electron Microscopy (SEM)

The examination of particle morphology was conducted using a scanning electron microscope (SEM). To get good image of SEM the necessary conditions are, accelerating voltage, working distance, spot size, and scan speed. The SEM images of AC/Iron oxide nanoparticle revealed the nanoparticles have spherical and nano disc like morphology with agglomeration, The agglomeration in the nanoparticles is due to the interaction of van der Waals interaction between the iron oxide nanoparticles [46] shown in (Fig. 2a, b).

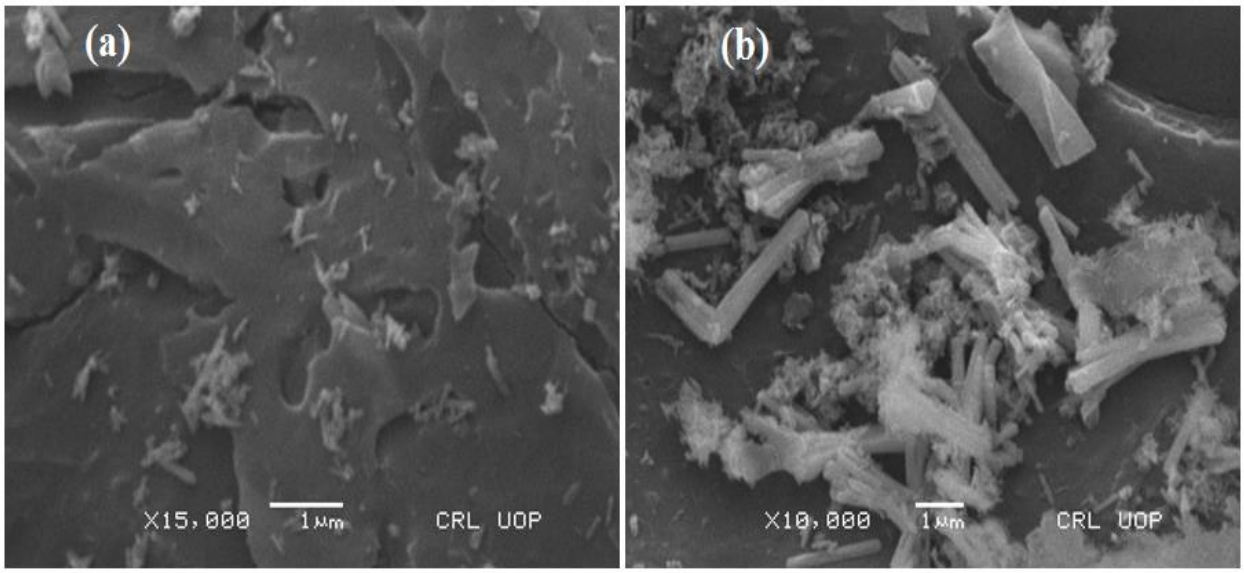

Figure 2. a, b. SEM micrograph of composite AC/Fe_2O_3 and activated carbon.

3.1.2. X-Rays Radiation Diffraction

The Fig. 3 illustrates the X-ray diffraction patterns of activated carbon and the AC/Fe_2O_3 composite. In the design of activated carbon, several prominent peak are observed at 2θ values of 25.0°, 36.25°, and 47.5°. These strong diffraction peaks indicate the creation of zinc oxide (ZnO) through carbonization. Impurities may be responsible for additional peaks in the pattern. A crystalline structure is confirmed by the XRD pattern's existence of sharp peaks. Furthermore the diffraction patterns of the AC/Fe_2O_3 composite closely resemble the conventional data for rhombohedral crystal hematite with diffraction peaks at 2θ values of 49.45° (024), 24.25°(012) and 35.65° (110) [47, 48].

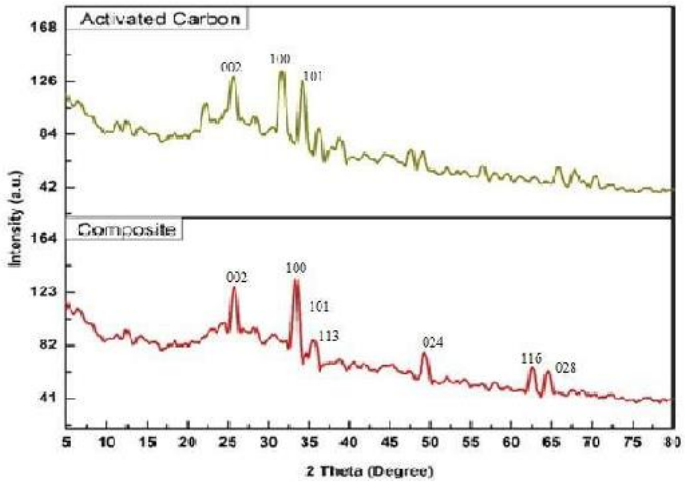

Figure 3. Activated Carbon and AC/Fe_2O_3 Composite XRD pattern.

3.1.3. Fourier Transform Infrared (FTIR) spectroscopy

The dipole change is required for Infra-red radiations absorption. The stretching of the C=CH_2 bond is shown by a unique peak in the spectra of activated carbon at 900 cm^{-1} [49] . Additionally, the bending of the aromatic C-C bond, =C-H bond, C=C bond and of alkene is responsible for the additional peaks at 868 cm^{-1}, 980 cm^{-1} and 1539 cm^{-1}respectively [50, 51] . The AC/Fe_2O_3 composite's spectra show there is a noticeable reduction in the intensity of bands between 500-1000 cm^{-1}, potentially indicating interaction between Fe_2O_3 and activated carbon [52]. Notably, the vibrational mode associated with the Fe-O bond is indicated by the peak observed at 521 cm^{-1} in the composite spectra of AC and Fe_2O_3 [53, 54].

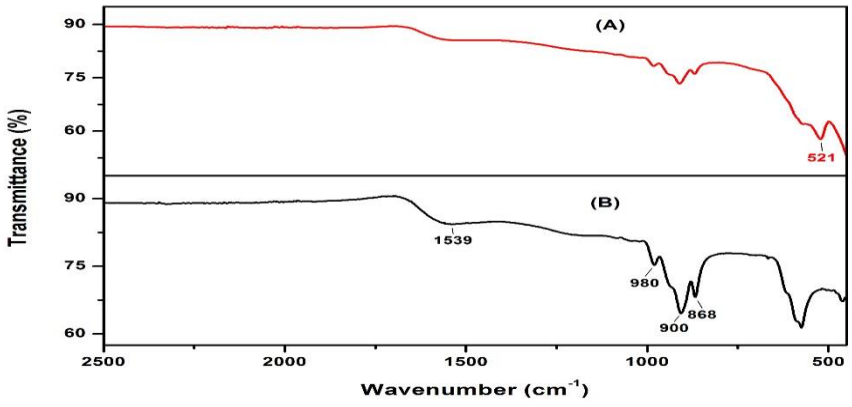

Figure 4. (A) Activated Carbon **(B)** AC/Fe_2O_3 Composite FTIR spectra.

3.1.4. Analysis Using Thermogravimetric

A thermogravimetric investigation was conducted to assess the stability of the AC/Fe_2O_3 composite, extending up to 700°C (Fig. 5). The degradation of Fe2O3/AC occurred in four distinct stages as indicated by the TGA peaks. The first weight loss (below 175 °C) was mainly due to the loss of moisture. A second peak at around 276 °C with very low weight loss (within 175–387 °C) was found due to the thermal degradation of cellulose and hemicellulose [55]. Between 387 and 700 °C, a third peak with a loss of 8.4% was due to the devolatilization of more thermally stable heavy volatiles present in Fe2O3/AC [46] .

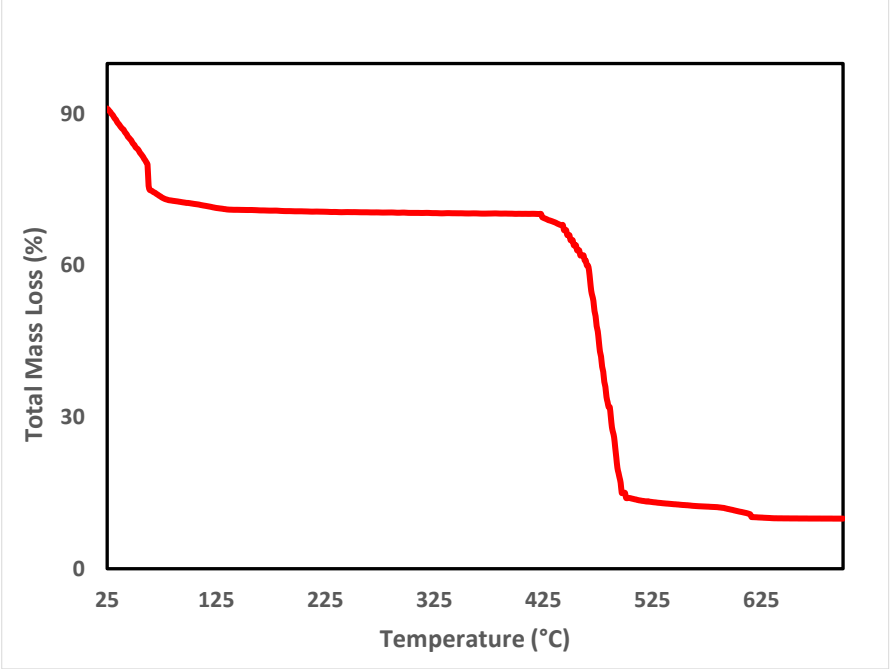

Figure 5. Composite AC/Fe_2O_3 TGA curve.

3.2. Batch adsorption studies

Batch mode tests were conducted by placing a defined quantity of adsorbate and sorbent in a culture tube and subjecting it to agitation, using a wrist-hand shaker. The study examined at how piroxicam-beta-cyclodextrin, paracetamol and diclofenac potassium adsorb to the AC/Fe_2O_3 composite and the effects of pH, contact time, temperature, adsorbent dosage and adsorbate concentration.

3.2.1. pH dependent studies

The pH of the solution plays a vital role in influencing the surface charges of the adsorbent and the protonation or deprotonation of functional groups present in pharmaceuticals. It is a critical factor in determining the interactions between the adsorbent and adsorbate [56]. To investigate this influence, we employed 0.1 g of adsorbent, 50 ppm of adsorbate, and maintained a contact duration of 60 minutes for each of the three painkillers. As shown in Fig. 6 (b) the highest adsorption for paracetamol occurred at pH 7, for diclofenac potassium at pH 4, and for piroxicam-beta-cyclodextrin at pH 2.

Adsorption of paracetamol showed an upward trend with rising pH, peaking at pH 7. At lower pH levels, both the carbonyl group in paracetamol and the activated carbon surface acquired a positive charge, while at elevated pH levels, the oxygen within the phenol group of paracetamols and the activated carbon surface exhibited negative charges. This led to electrostatic repulsion between similarly charged species at both low and high pH values, thereby reducing adsorption [57, 58]. Conversely, due to the heightened water solubility of diclofenac potassium, elevating the pH above 4.0 led to a declining trend in the adsorption of diclofenac potassium [59]. Conversely, piroxicam-beta-cyclodextrin exhibited high solubility in neutral and high-pH conditions, thereby enhancing adsorption at low pH levels, such as pH 2 [60, 61].

3.2.3. Effect of adsorbent dosage

We investigated the impact of varying the adsorbent dose on the adsorption of diclofenac potassium, piroxicam-beta-cyclodextrin, and paracetamol within the dosage range of 0.02-0.14 g/10mL for diclofenac potassium and paracetamol. although for piroxicam-beta-cyclodextrin, it was investigated within the range of 0.001-0.2 g/10mL, all under optimized pH and contact time conditions [55]. The findings show that for paracetamol, diclofenac potassium, and piroxicam-beta-cyclodextrin, respectively, adsorption increased up to 0.1g, 0.06g, and 0.05g, achieving maximum adsorption rates of 95%, 96%, and 87% respectively, and thereafter remained largely constant. The rise in the quantity of adsorbent led to a rise in active sites on the adsorbent surface, resulting in increased painkiller adsorption [62].

3.2.4. Adsorbate concentration's influence

Under optimal circumstances, the impact of adsorbate concentration (Diclofenac potassium, Piroxicam-beta-cyclodextrin, and Paracetamol) was investigated over concentration ranges spanning from 25 ppm to 200 ppm. Due to the limited number of available adsorption sites on the adsorbent, the outcomes illustrate a reduction in the percentage of adsorption. [63]. Interestingly, for all painkillers, a maximum percent adsorption of 25 ppm was noted **Fig. 6 (a)**

Various isotherm models were employed to scrutinize the experimental findings and gain insights into the adsorption mechanism.

Adsorption can manifest in multiple locations, as indicated by the Freundlich isotherm model [64] revealing the heterogeneity of the adsorbent surface [64]. This model assumes an infinite surface coverage, as it does not consider the adsorbate's potential to entirely envelop the adsorbent's surface. The linear representation of the Freundlich isotherm model was applied:

$$\log qe = \frac{1}{n}\log C_e + \log K_F \qquad (4)$$

In this examination, KF signifies the utmost adsorption capacity, whereas 1/n reflects the adsorption strength. Equilibrium adsorbate concentration is denoted as Ce, and the quantity of adsorbate adsorbed per gram is represented as qe [140,141]. The experimental data were subjected to scrutiny using the Freundlich isotherm model, and the outcomes are show cased in Figure 6 (e). It is discernible that the Freundlich model offers the most optimal fit for diclofenac potassium and paracetamol, boasting R^2 values of 0.9983 and 0.995, respectively. By calculating the slope of the graph, we were able to ascertain the Freundlich constant. Freundlich adsorption model assumes that adsorbents have a heterogeneous surface having sites with different adsorption potential. It also assumes that stronger binding sites are occupied first and the binding strength decreases with the increasing degree of occupation.

We employed the Langmuir isotherm model to elucidate the formation of a monolayer adsorbate on the adsorbent surface [65]. According to this model, the adsorbent's surface comprises uniform active sites that establish chemical bonds with the adsorbate. The isotherm was expressed linearly as follows:

$$\frac{C_e}{q_e} = \frac{1}{KL} + aL\frac{C_e}{KL} \qquad (5)$$

In this context, qe signifies the adsorbate quantity adsorbed (in mg g^{-1}), Ce represents the equilibrium adsorbate amount (in mg L-1), and aL and KL denote the Langmuir constants, signifying the strength of bonds and the utmost adsorption capacity, respectively.

For each of the three painkillers, a Ce versus Ce/qe plot was created; the outcomes are shown in Fig. 6 (d). The criterion for favorable adsorption was chosen on the basis of RL values. If RL values are greater than 1.0, adsorption is unfavorable, if RL values are equal to 1.0, adsorption is linear, if RL values are between 0 and 1, adsorption is favorable and if RL values are equal to 0, adsorption is irreversible. For the present system, the RL values were between 0 and 1 (0.01–0.919) for all the adsorbates to the nanoparticles indicating favorable adsorption process (Table 1).

Using the Temkin isotherm [100], which proposes that the decrease in the heat of adsorption follows a linear pattern rather than a logarithmic one as a function of coverage, we conducted further analysis. This analysis revealed a linear reduction in the heat of adsorption due to interactions between the adsorbent and adsorbate [66]. The linear form of this model is expressed as follows:

$$q_e = BlnQ_T + BlnC_e \quad (6)$$

where $B = RT/bT$ (7)

In this equation, the symbols are described as follows:

bT denotes the Temkin isotherm constant.

R represents the Ideal Gas Constant (8.314 J/mol/K).
K_T signifies the Equilibrium Binding Constant (L/g).
B is a constant linked to the heat of adsorption (J/mol).
Fig. 6 (c) display the graphs of qe versus lnCe for the painkillers. Concurrently, Table 1 provide the respective constants bT and KT, along with the correlation coefficients for the Temkin isotherm concerning diclofenac potassium, piroxicam-beta-cyclodextrin, and paracetamol.
Despite fluctuations in temperature, we employed the Dubinin-Radushkevich isotherm model [67] to assess the surface energy heterogeneity [68]. It is said to be expressed like follows:

$$lnqe = lnQm - k\varepsilon^2 \quad (8)$$

In this equation, the Polanyi potential is denoted as ε, Qm signifies the maximum adsorption capacity (mg g^{-1}), Qe represents the equilibrium adsorption, and k is the Dubinin-Radushkevich constant [69]. One way to express the Polanyi potential (ε) is as follows:

$$\varepsilon = RTln\left(1 + \frac{1}{C_e}\right) \quad (9)$$

In the provided equation, R stands for the ideal gas constant (8.314 J mol-1 K-1), T represents the absolute temperature (K), and Ce denotes the equilibrium concentration (mg L-1). This model utilizes the free energy of adsorption to differentiate between physisorption and chemisorption, and it can be computed using the following equation:

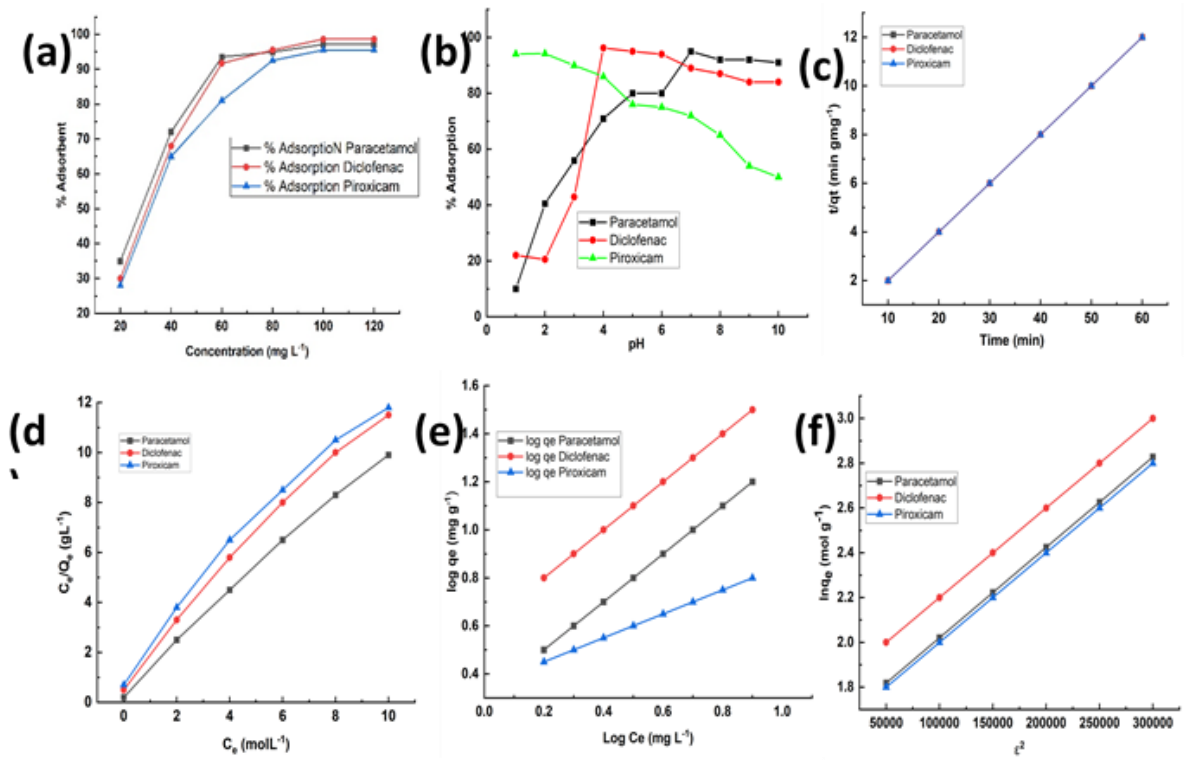

Figure 6. (a) Effect of Concentration, (b) pH, (c) Temkin model, (d) Langmuir Isotherm, (e) Freundlich Isotherm and (f) D-R Model for the adsorption of adsorbates on the adsorbent.

Table 1. The isotherm models, parameters for the adsorption of paracetamol, diclofenac potassium and piroxicam-beta-cyclodextrin on the AC/Fe_2O_3 composite.

Model	Parameters	Paracetamol	Diclofenac Potassium	piroxicam-beta-cyclodextrin
	Q_{max}(mg g-1)	1.9896538	8.474576	72.9927
	K_L (mg g-1)	77.72085	327.2037	71.7232

Langmuir	**R_L** (dm^3mol^{-1})	0.388	0.1636	0.3583
	R^2	0.9805	0.9564	0.9705
Freun-dlich	**1/n**	0.7796	0.7479	-0.3382
	K_f(mg g-1)	2.139439	6.635903	8.308067
	R^2	0.995	0.9983	0.9136
Temkin	**bT**	8.4549	9.1357	9.4672
	K_T(Lg^{-1})	0.490464	1.822554	0.256319
	R^2	0.9868	0.9953	0.9938
Dubnin-Radush-kevich	***Q_m***(mg g-1)	1.046300932	1.094437	1.054521
	E($kJmol^{-1}$)	353.5533906	1000	223.6067977
	R^2	0.9016	0.9555	0.9449

Table 2

Capacities of NSAIDs adsorption onto ACs from various wastes

Precursor	Adsorbate	C_o (mg/l)	q_L (mg/g)	Ref.
Cork waste	IBP	20e120	416.7	[70]
Olive stones	IBP	5e100	160.9	[71]
Olive stones	IBP	5e100	282.6	[71]
Waste apricot	NPX	100e500	106.4	[72]
Banana peels	Paracetamol	75 mg/L	160	Present
Banana peels	Diclofenac po-tassium	50 mg /L	165	Present
Banana peels	Piroxicam-beta-cyclodex-trin	70 mg/L	170	Present

3.2.2. Time dependent study.

Over a time, span ranging from 10 to 90 minutes, we investigated the impact of contact time on the adsorption of painkillers onto AC/Fe_2O_3, while maintaining consistent quantities of adsorbent (0.1g), adsorbate concentration (50 ppm), and the pH conditions that were previously optimized. All of painkillers that were studied, the percentage of adsorption increased with extended contact time, a phenomenon attributable to the porous structures and active sites present within the AC/Fe_2O_3 composite [73, 74].

Equilibrium, signifying the point at which adsorption remained constant, was reached at different time intervals for each painkiller. Specifically, equilibrium was attained at 30 minutes for diclofenac potassium, 40 minutes for paracetamol, and 50 minutes for piroxicam-beta-cyclodextrin, as illustrated in Figure 7 (a). These optimal durations were deemed optimal for follow-up experiments.

Kinetic models, which are models describing motion, serve as pivotal tools in elucidating the adsorption mechanism. They provide insights into mass transfer and the step that determines the rate involved in the process [75]. In the present investigation, we explored and examined the adsorption mechanisms of painkillers onto the AC/Fe_2O_3 composite. To accomplish this, we employed a range of kinetic models, which encompassed the Reichenberg, Webber-Morris, as well as the pseudo-first-order and pseudo-second-order models [76, 77]

The Lagergren pseudo-first-order model can be represented by the following linear equation. [92].

$$\log Q_c - Q_t = \log Q_c - \frac{K_t}{2.303} \quad (11$$

Within this model, Qt represents the adsorbate quantity adsorbed at time t, K is the rate constant, and Qe signifies the adsorbate quantity adsorbed at equilibrium. The pseudo-first-order kinetic model assumes that the rate of occupation of adsorption sites is proportional to the number of unoccupied sites [78]. For diclofenac potassium, piroxicam-beta-cyclodextrin, and paracetamol, the adsorption data did not exhibit a favorable match with the pseudo-first-order model when assessing the plot of log(Qe - Qt) against time t. The linear form presented below was utilized to employ the pseudo-2nd-order model [79]:

$$\frac{t}{Q_t} = \frac{t}{Q_e} + \frac{1}{K_2 Q_{e^2}} \quad (12)$$

In this context, Qt signifies the adsorption at a given time t, while Qe represents the adsorption at equilibrium, and K_2 stands for the rate constant of the pseudo-second-order model. The adsorption of paracetamol, diclofenac potassium, and piroxicam-beta-cyclodextrin onto the AC/Fe_2O_3 composite adhered to the pseudo-second-order model, as evident from the t/Qt vs. t graphs Fig. 7 (c).
The adsorption information was subjected to analysis using the Webber-Morris kinetic model[80] to discern whether the rate-controlling step was attributed to film or intraparticle diffusion.
The following is how the Webber-Morris kinetic model is expressed:

$$Qt = R_d t^{1/2} \quad (13)$$

Within this equation, Qt represents the quantity of adsorbate adsorbed at a specific time interval, while Rd signifies the rate of intraparticle diffusion, derivable from the slope [80]. When intraparticle diffusion plays a role in the adsorption process, the plots of Qt against the square root of time (t½) should result in linear graphs. These graphical representations are showcased in Figure S1 (c). Interestingly, it can be inferred that intraparticle diffusion is not the limiting step for diclofenac potassium and paracetamol, as the linear plots do not intersect the origin. On the contrary, the variance observed for piroxicam-beta-cyclodextrin indicates that intraparticle diffusion is indeed the rate-controlling step in this case. The constants are listed in Table S1 and were determined from the charts.
A simple equation was developed by Reichenberg [95] to clarify the mechanics underlying the adsorption process [81]. This model can identify whether intraparticle diffusion or film diffusion contributes to the adsorption process. The utilization of this model is articulated as follows:

$$Q = 1 - \frac{6e^{-Bt}}{\pi^2} \quad (14)$$

In this context, Qt represents the quantity of adsorbate adsorbed at a specific time t, and Qe represents the maximum adsorption capacity. It can be expressed as Q = Qt/Qe. Following is how Bt is calculated:

$$Bt = -0.4977 - \ln(1 - Q) \quad (15)$$

Fig. 7 (b) displays the outcomes, and it's evident from the linear plots that they do not meet at **t**he origin, which suggests the formation of a thin adsorbate layer on the surface of the AC/Fe_2O_3 composite.

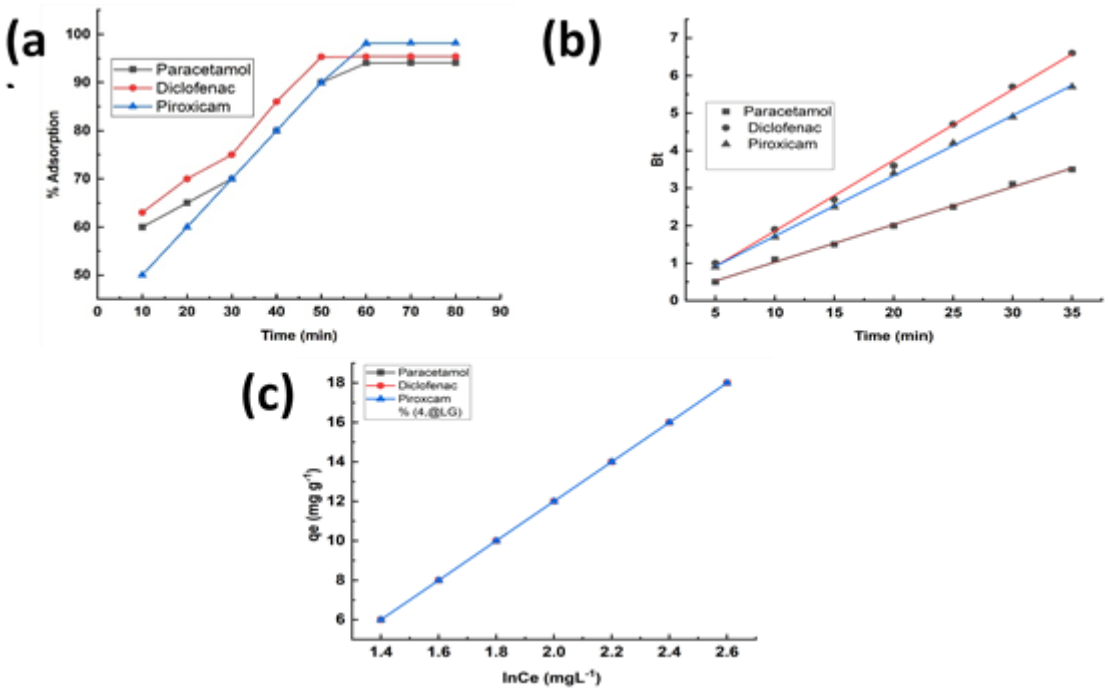

Figure 7. (a) Contact Time Influence, (b) Reichenberg Model (c) Pseudo-second-order model.

3.2.5. Temperature Effect

In an ideal setting, we investigated the influence of temperature on the adsorption of diclofenac potassium, piroxicam-beta-cyclodextrin, and paracetamol onto the AC/Fe_2O_3 composite within the temperature range of 283K to 333K. The outcomes reveal that with rising temperature, the adsorption capacity experiences a reduction. This decline in adsorption at elevated temperatures could be attributed to the increased solubility of the adsorbate, which promotes stronger interactions between the adsorbate and the solvent, potentially outweighing interactions with the adsorbent [82, 83]. Fig. 8 (a)

3.2.5 Thermodynamic principles

The experimental results were run through the following thermodynamic equations to determine various parameters, such as entropy, enthalpy, and free energy [84, 85].

$$\Delta G° = -RTlnKc \qquad (16)$$

$$\Delta G° = \Delta H - T\Delta S \qquad (17)$$

$$lnKc = \frac{\Delta S°}{R} - \frac{\Delta H}{RT} \qquad (18)$$

Within the presented equations, ΔG° stands for Gibbs free energy (kJ mol $^{-1}$), ΔH represents the enthalpy change (kJ mol^{-1}), ΔS denotes the entropy change (J K^{-1}), the ideal gas constant (R) is 8.314 J mol-1 K-1, and temperature is indicated as T (K). The following equation can be used to calculate the equilibrium constant (Kc).

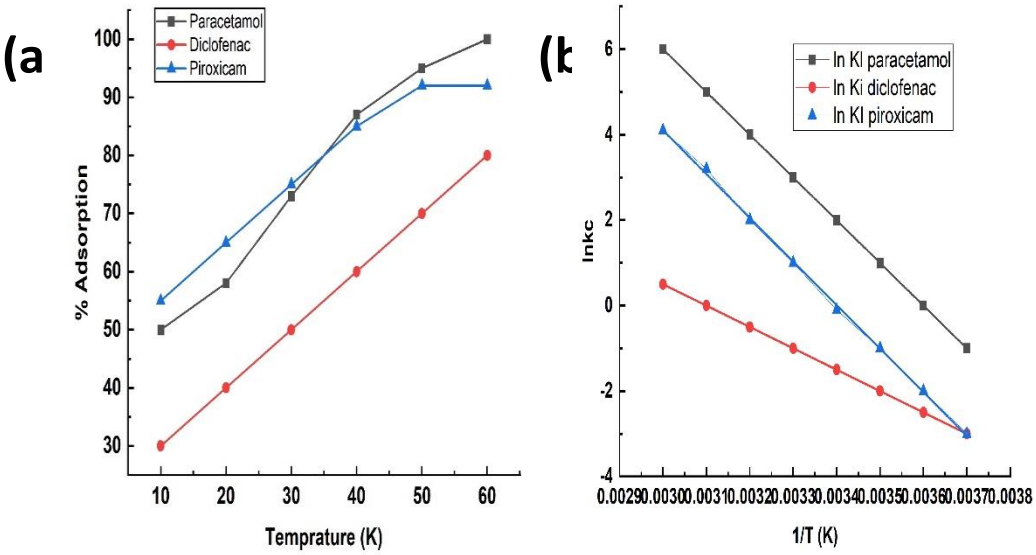

Figure 8. (a) Temperature-dependent, (b) Vant Hoff Equation.

$$Kc = \frac{F}{1-F} \qquad (19)$$

Where F is the amount of adsorbate adsorbed on the adsorbent of the solution at equilibrium (mol dm^{-3}), while 1-F, the equilibrium concentration of the adsorbate in the solution (mol dm^{-3}) [86].

For each painkiller, plots of Kc against 1/T were created. Fig. 8 (b) shows these results graphically. The deduction that the process is both spontaneous and exothermic is substantiated by the values of Gibbs free energy (ΔG°) and enthalpy (ΔH).

Table 3. The thermodynamic factor affecting the adsorption of piroxicam-beta-cyclodextrin, diclofenac potassium, and paracetamol onto AC/$F_{e2}O_3$ composite.

Adsorbate	**ΔH (KJ mol $^{-1}$)**	**ΔG° (KJ mol $^{-1}$)**	**ΔS (J K^{-1})**
Paracetamol	-68.825786	-6.85768122	-217.219878
Diclofenac potassium	-63.0359166	-1.06892571	-167.793148
Piroxicam-beta-cyclodextrin	-10.8863516	-0.92771421	-35.1075278

Table 4. Thermodynamic parameters of NSAIDs adsorption onto ACs from different wastes.

Precursor	Adsorbate	ΔH° (J/mol)	ΔS° (J/mol.K)	ΔG° (J/mol)			Adsorption nature	Ref.
				303 K	313 K	323 K		

Magwort leaves	IBP	57.45	198.16	1.745 3.297 5.728	Endothermic	[87]
Mung bean husk	IBP	—42.13	—104.7	11.64 9.59	Exothermic	[88]
Parthenium weed	IBP	—50.81	—158.2	2.198 3.735 4.459	Exothermic	[88]
Bone char	IBP	—50.45	—146.08	5.65 3.28 2.97	Exothermic	[89]
Cyclamen tubers	DCF	—17.45	—50.08	2.55 1.97 1.55	Exothermic	[90]
Banana peels	Paracetamol	-68.825786	-217.219878	-6.85768122	Exothermic	Present
Banana peels	Diclofenac potassium	-63.0359166	-167.793148	-1.06892571	Exothermic	Present
Banana peels	Piroxicam-beta-cyclodextrin	-10.8863516	-35.1075278	-0.92771421	Exothermic	Present

3.3. DFT Conclusions

3.3.1. Composite of AC and Fe_2O_3

In addition to the experimental results, computer simulations were used to investigate several painkiller adsorption configurations on the AC/Fe_2O_3 composite. Figs S 2 and S 3 show the optimal geometries of the Fe_2O_3 cluster, and activated carbon. Alcoholic and CH_2 groups, as well as aromatic rings, were found on activated carbon, according to the FTIR results. Consequently, a graphitic structure of activated carbon with functional groups, resemble to OH and COOH on its surface was modelled.

Fe_2O_3 was built into a compact cluster-like structure, per the experimental characterization. At first, the geometries of the Fe_2O_3 monomers and activated carbon were individually optimized. These monomers were then combined to create a composite, which was then optimized. After optimization, it was clear that Fe_2O_3 solidly attached to the surface of the activated carbon by forming strong intermolecular connections with it. At a distance of 1.82 Å between the atoms, the oxygen atom in Fe_2O_3 established a robust intermolecular hydrogen bond with the OH functional group situated on the surface of the activated carbon.

Furthermore, a robust chemical bonding occurred between the oxygen atom of the activated carbon and the iron (Fe) atom of Fe_2O_3, leading to an increased binding energy of -2.34 eV. This reduced binding energy illustrates the energetically favorable nature of AC/Fe_2O_3 composite formation. Additionally, there was a transfer of 0.18 electron charges from the Fe atom to the O atom within the functional group, along with a transfer of 0.089 electron charges from the hydrogen atom of the OH functional group to the oxygen atom of Fe_2O_3.

3.3.2. Adsorption of painkillers onto the composite AC/Fe_2O_3

To gain a comprehensive insight into the interactions between the painkillers and the diverse active sites within the composite material, multiple adsorption configurations were individually examined for each of the painkillers.

3.3.2.1. Adsorption of paracetamol onto the AC/Fe_2O_3 composite

For the investigation of paracetamol adsorption, three distinct adsorption modes were employed. In Complex-1 (CMP-1), a robust intermolecular hydrogen bond (OH---O) with a bond length of 1.82 Å was established between the OH group of paracetamol and the oxygen (O) atom of Fe_2O_3, facilitating their interaction within the Fe_2O_3 composite [91]. This configuration's predicted adsorption energy of -18.92 kcal/mol suggests the creation of a stable compound. In addition, 0.11 electrons were transferred from the paracetamol hydrogen atom to the Fe_2O_3 oxygen atom [92].

Paracetamol interacted with the composite in Complex-2 (CMP-2) at two different sites: the NH site and the CH site of the aromatic ring. Paracetamol and the composite had weak van der Waals interactions, with bond lengths of 2.73 Å and 2.86Å, according to geometry optimization [93]. This complex's computed adsorption energy of -6.34 kcal/mol points to physisorption. An examination of charge transfer revealed that there was little electron transfer between the adsorbent and adsorbate.
Paracetamol engaged with Complex-3 (CMP-3) through its C=O site, where the oxygen (O) atom within the C=O bond established a potent connection with the iron (Fe) atom of Fe_2O_3. A 2.00Å bond length robust bond was formed as a result of geometry optimization. In comparison to CMP-1 and CMP-2, this combination formed with the lowest adsorption energy, at -24.33 kcal/mol. Charge transfer analysis revealed a significant transfer of 0.23 electrons from the iron (Fe) atom of Fe_2O_3 to the oxygen (O) atom within the C=O group of paracetamol [94].

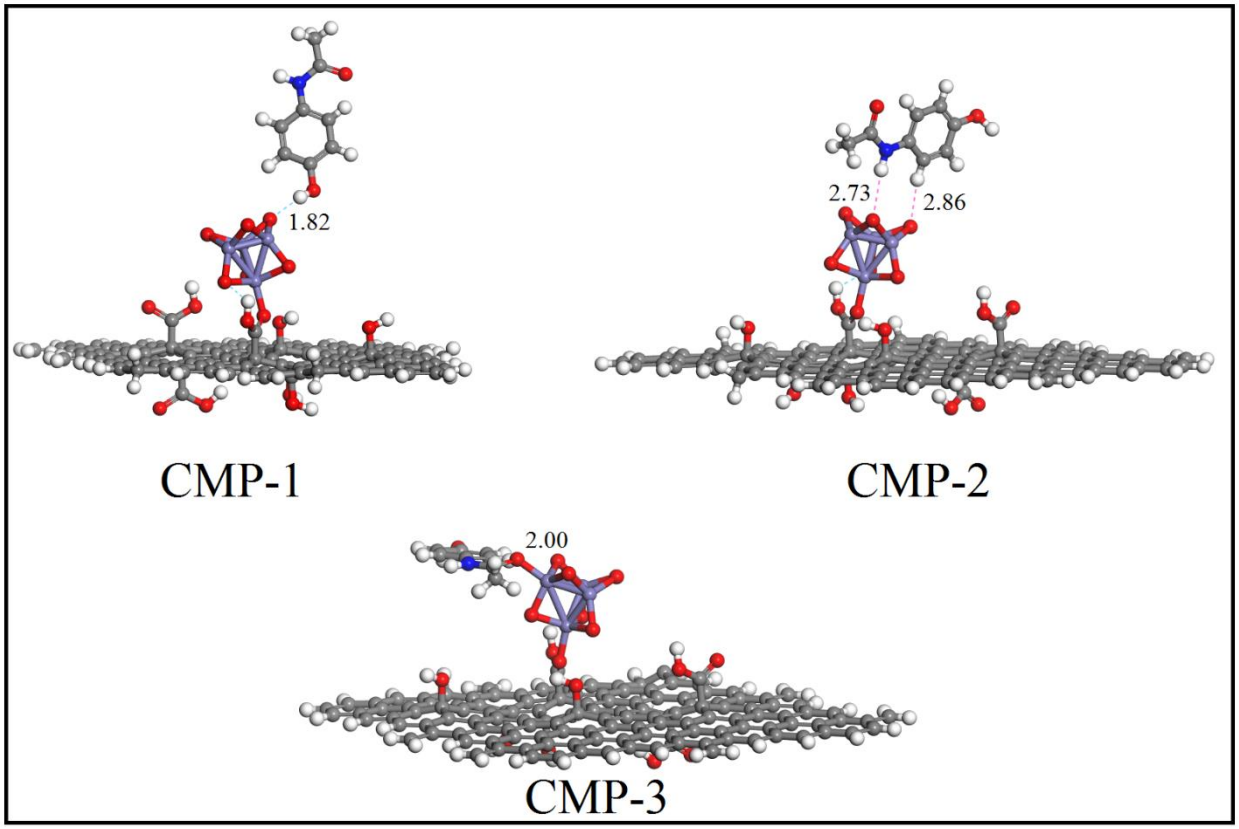

Figure 9. Paracetamol adsorption over an AC/Fe_2O_3 composite has been optimized using multiple adsorption configuration geometries. Bond radii are displayed in Å.

3.3.2.2. Adsorption of Diclofenac Potassium on an AC/Fe_2O_3 Composite

For the examination of diclofenac potassium adsorption, three distinct adsorption modes were explored. In Complex-1 (CMP-1), the two oxygen (O) atoms of Fe_2O_3 formed connections with the two CH groups of the aromatic ring of diclofenac [95]. Diclofenac and the Fe_2O_3 composite had modest intermolecular interactions, as revealed by geometry relaxation, with bond lengths of 2.83 Å and 2.60 Å [95]. The physisorption character of this configuration was shown by the predicted adsorption energy of -8.43 kcal/mol. According to charge transfer studies, 0.02 and 0.04 electrons were transferred from the diclofenac H atom to the Fe_2O_3, O atoms [96].
Diclofenac interacts with the composite in Complex-2 (CMP-2) via the Cl atom of its aromatic ring, with a bond distance of 2.75 Å, geometry optimization revealed weak van der Waals interactions between diclofenac and the composite. This complex's computed adsorption energy was -5.64 kcal/mol, which denotes poorer adsorption. An examination of charge transfer found that there was little electron transfer between the adsorbent and adsorbate [97].
Diclofenac engaged in interactions with Complex-3 (CMP-3) through its C=O, NH, and Cl sites. At a bond length of 2.60 Å, the oxygen (O) atom within diclofenac's C=O linkage and the iron (Fe) atom of Fe_2O_3 established a relatively weak bond. The chlorine (Cl) atoms interacted via van der Waals interactions with the Fe and O atoms

of Fe_2O_3, with bond lengths of 2.68 Å and 2.90 Å, respectively. Additionally, the hydrogen atom of the NH group formed a connection of 2.61 Å with the oxygen atom of Fe_2O_3. The adsorption energy value for this complex was -8.72 kcal/mol, indicative of physisorption. Charge transfer studies revealed a substantial transfer of 0.01 to 0.03 electrons between the adsorbent and the adsorbate [97].

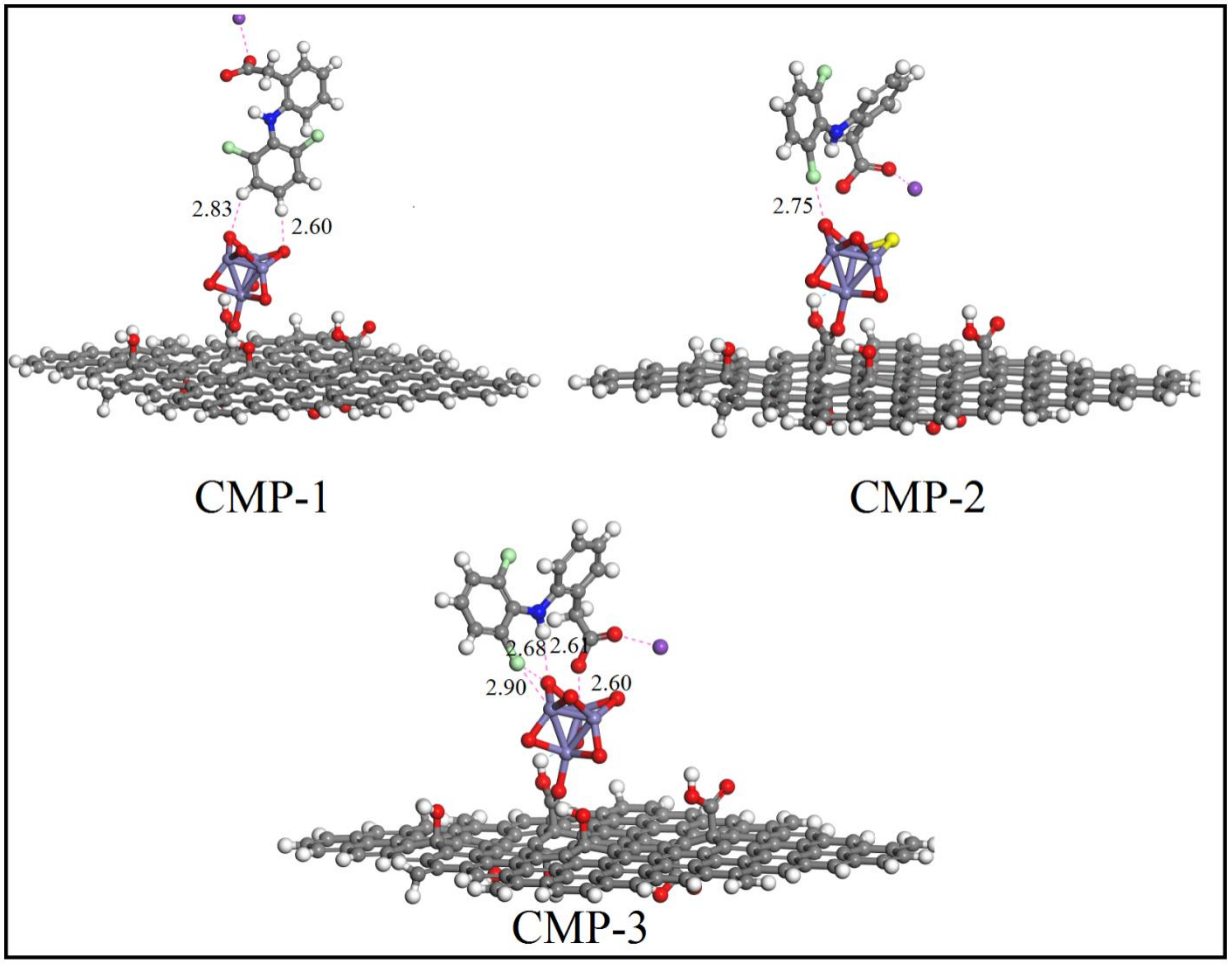

Figure 10. Diclofenac adsorption over an AC/Fe_2O_3 composite has been optimized for various adsorption configuration geometries. The symbol for a bond distance is Å.

3.3.2.3 Adsorption of Piroxicam-Beta-Cyclodextrin on the AC/Fe2O3 Composite.

As shown in Fig. 11, the compound in the instance of piroxicam-beta-cyclodextrin is made up of two groups: piroxicam and beta-cyclodextrin. Separate adsorption simulations were run for these two groups in order to reduce computing time and guarantee precise interaction modelling [98]. Four different adsorption arrangements, designated CMP-1 to CMP-4, were looked at for piroxicam.

Piroxicam engaged with the Fe_2O_3 site of the composite in CMP-1 through its OH site. The hydrogen atom of the OH group in piroxicam formed a hydrogen bond with the oxygen atom of Fe_2O_3, as indicated by geometry optimization, with a bond distance of 1.85 Å. This complex's adsorption energy, which was -15.34 kcal/mol, suggested a robust interaction. According to a charge transfer investigation, the H atom of piroxicam transferred 0.10 electrons to the oxygen atom of Fe_2O_3 [99].

Piroxicam's NH group and the H-atoms in its methyl group established interactions with Fe_2O_3 in CMP-2. Geometry optimization revealed that the H atoms of the methyl group formed bonds with an average length of 3.47 Å, while the H atom of the NH group established a bond with a length of 3.65 Å. The adsorption energy for this compound was estimated to be -4.31 kcal/mol, and there was minimal charge transfer during complexation. Piroxicam interacted with the composite in CMP-3 and CMP-4 through the SO_2 group and the oxygen (O) atom of the C=O bond. Geometry optimization demonstrated that the O atom formed strong chemical connections with the composite in both complexes, with bond distances of 2.12 Å and 2.00 Å for C=O—Fe and SO—Fe, respectively.

This is evidenced by the substantial chemisorption indicated by adsorption energies of -21.41 kcal/mol for CMP-4 and -23.51 kcal/mol for CMP-3. According to a Hirshfeld charge transfer analysis, CMP-3 and CMP-4 transferred 0.21 and 0.19 electrons, respectively.

There was just one adsorption mode, CMP-5, taken into account for the beta-cyclodextrin group. In this arrangement, the beta-cyclodextrin's two OH groups interacted with the composite's Fe_2O_3 site's two oxygen atoms. With bond distances of 2.65 Å and 2.81 Å, respectively, geometry optimization showed reduced intermolecular interactions between beta-cyclodextrin sites and the composite [100]. This complex's adsorption energy of -6.14 kcal/mol points to physisorption. These simulations showed that, in contrast to the beta-cyclodextrin site, the piroxicam-beta-cyclodextrin site strongly interacted during the removal process.

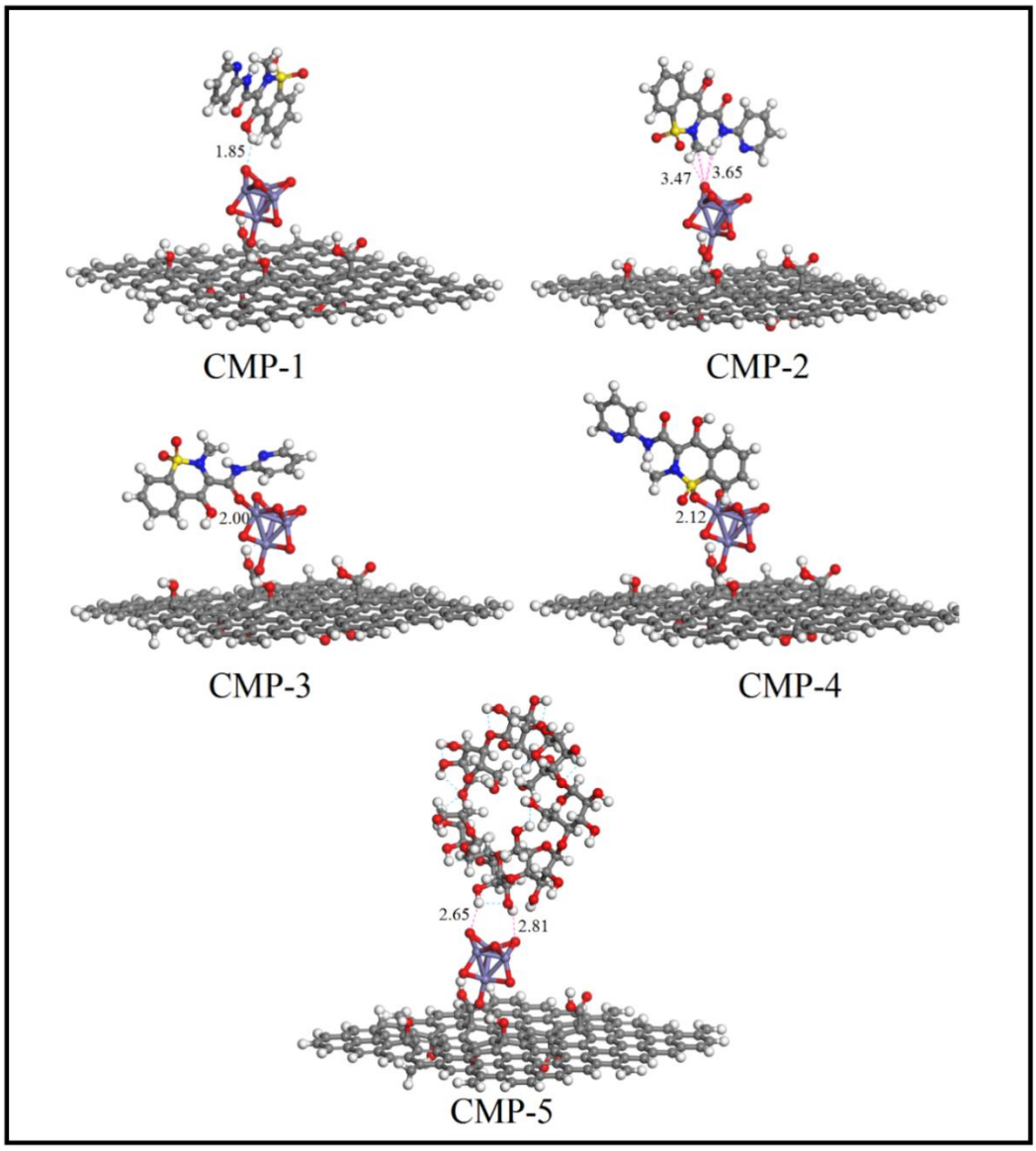

Figure 11. Piroxicam and beta cyclodextrin adsorption on AC/Fe_2O_3 composite optimized geometries of varied adsorption configuration. Bond radii are displayed in **Å**.

4. Conclusion

In this study, a stable magnetic AC/Fe_2O_3 nanocomposite was synthesised without using highly toxic chemicals. This technique is also suitable for preparing similar carbon–metal oxide nanocomposite using transition and inner-transition metal salts. The AC/Fe2O3 nanocomposite possesses excellent magnetic properties and Fe2O3 in

carbon matrix is in nano-size with uniform morphology. Moreover, they are attracted by permanent magnet in water which makes easy way to separate water from carbon adsorbed with NSAIDs. Hence this magnetic composite would be a promising material in adsorption technology, and SEM, XRD and FTIR investigations were used to establish its chemical composition. Diclofenac potassium, piroxicam-beta-cyclodextrin, and paracetamol were all removed from water using this composite. The comprehensive optimization of various adsorption-related factors, encompassing contact time, pH, adsorbent dosage, temperature, and adsorbate concentration. Notably, the greatest adsorption capabilities for paracetamol were attained at pH 7 (92.9%), diclofenac potassium at pH 4 (96.2%), and piroxicam-beta-cyclodextrin at pH 2 (94.2%). Various models, including Langmuir, Freundlich, Dubinin-Radushkevich (D-R), and Temkin isotherm, were meticulously employed to delve into the adsorption mechanism. The Freundlich isotherm model, which had high linear regression coefficients of 0.995 and 0.9983, respectively, produced notable fits for paracetamol and diclofenac potassium. On the other hand, the adsorption equilibrium results for piroxicam-beta-cyclodextrin were more clearly explained by the Temkin isotherm model. The pseudo-second-order model, notably, yielded the most optimal fit for the kinetic data of all painkillers. Interestingly, temperature-dependent adsorption studies allowed for the determination of thermodynamic parameters, including ΔH (enthalpy change), ΔS (entropy change), and ΔG (Gibbs free energy change). The results demonstrated that all of the analgesics adsorb exothermically and spontaneously onto the AC/Fe_2O_3 composite. Moreover, density functional theory (DFT) calculations were conducted to examine the adsorption of painkillers on the AC/Fe_2O_3 composite. These simulations revealed substantial interactions with the Fe_2O_3 site of the composite across various adsorption configurations. With an adsorption energy of -24.33 kcal/mol, CMP-3 was found to be the most stable adsorption configuration for paracetamol. Diclofenac exhibited robust interactions in both the CMP-1 and CMP-3 adsorption configurations. In contrast, piroxicam-beta-cyclodextrin displayed strong intermolecular bonds and higher adsorption energies of -23.51 and -21.47 kcal/mol, respectively, with Fe_2O_3 at its C=O and SO_2 sites.

Conflicts of Interests: The authors declare no conflict of interests.

References

1. Shamsudin, M.S., et al., *Fabrication and characterization of a thin coated adsorbent for antibiotic and analgesic adsorption: Experimental investigation and statistical physical modelling.* Chemical Engineering Journal, 2020. **401**: p. 126007.
2. Lima, E.C., *Removal of emerging contaminants from the environment by adsorption.* Ecotoxicology and environmental safety, 2018. **150**: p. 1-17.
3. Spaltro, A., et al., *Removal of paracetamol from aqueous solution by activated carbon and silica. Experimental and computational study.* Journal of Contaminant Hydrology, 2021. **236**: p. 103739.
4. Lapworth, D., et al., *Emerging organic contaminants in groundwater: a review of sources, fate and occurrence.* Environmental pollution, 2012. **163**: p. 287-303.
5. Kansal, S.K. and A. Kumari, *Potential of M. oleifera for the treatment of water and wastewater.* Chemical reviews, 2014. **114**(9): p. 4993-5010.
6. Marques, S.C., et al., *Pharmaceuticals removal by activated carbons: Role of morphology on cyclic thermal regeneration.* Chemical Engineering Journal, 2017. **321**: p. 233-244.
7. Daughton, C.G., *Pharmaceuticals and personal care products in the environment: overarching issues and overview*. 2001, ACS Publications.
8. Sajid, M., et al., *Adsorption characteristics of paracetamol removal onto activated carbon prepared from Cannabis sativum Hemp.* Alexandria Engineering Journal, 2022. **61**(9): p. 7203-7212.
9. Wells, M.J., et al., *Emerging pollutants.* Water Environment Research, 2010. **82**(10): p. 2095-2170.
10. Sajid, M., et al., *Adsorption characteristics of paracetamol removal onto activated carbon prepared from Cannabis.* 2021.
11. Bond, C. and P. Hannaford, *Issues related to monitoring the safety of over-the-counter (OTC) medicines.* Drug Safety, 2003. **26**: p. 1065-1074.

12. Angeles, L.F., et al., *Assessing pharmaceutical removal and reduction in toxicity provided by advanced wastewater treatment systems.* Environmental Science: Water Research & Technology, 2020. **6**(1): p. 62-77.
13. Hejna, M., D. Kapuścińska, and A. Aksmann, *Pharmaceuticals in the aquatic environment: A review on eco-toxicology and the remediation potential of algae.* International Journal of Environmental Research and Public Health, 2022. **19**(13): p. 7717.
14. Kamaraj, R., N. Nesakumar, and S. Vasudevan, *Nitrogen Doped Carbon Nanomaterial as Electrocatalyst for Oxygen Reduction Reaction in Acidic Media: To use in Electro-Fenton.* ChemistrySelect, 2020. **5**(32): p. 10034-10040.
15. Luo, Y., et al., *A review on the occurrence of micropollutants in the aquatic environment and their fate and removal during wastewater treatment.* Science of the total environment, 2014. **473**: p. 619-641.
16. Carabineiro, S., et al., *Adsorption of ciprofloxacin on surface-modified carbon materials.* Water research, 2011. **45**(15): p. 4583-4591.
17. Rashed, M.N., *Adsorption technique for the removal of organic pollutants from water and wastewater.* Organic pollutants-monitoring, risk and treatment, 2013. **7**: p. 167-194.
18. Kusrini, E., et al., *Kinetics, isotherm, thermodynamic and bioperformance of defluoridation of water using praseodymium-modified chitosan.* Journal of Environmental Chemical Engineering, 2019. **7**(6): p. 103498.
19. Ashrul Asbollah, M., et al., *Individual and competitive adsorption of negatively charged Acid Blue 25 and Acid Red 1 onto Raw Indonesian kaolin clay.* Arabian Journal for Science and Engineering, 2022. **47**(5): p. 6617-6630.
20. Shafaati, M., et al., *The use of chitosan/Fe3O4 grafted graphene oxide for effective adsorption of rifampicin from water samples.* Research on Chemical Intermediates, 2020. **46**(12): p. 5231-5254.
21. Huang, L., et al., *Improved adsorption of streptomycin onto Thalia dealbata activated carbon modified by sodium thiosulfate.* Desalination and Water Treatment, 2015. **53**(6): p. 1699-1709.
22. Reza, R.A., et al., *Comparative adsorption behavior of ibuprofen and clofibric acid onto microwave assisted activated bamboo waste.* Industrial & Engineering Chemistry Research, 2014. **53**(22): p. 9331-9339.
23. Shahrin, E.W.E., et al., *Pectin derived from pomelo pith as a superior adsorbent to remove toxic Acid Blue 25 from aqueous solution.* Carbohydrate Polymer Technologies and Applications, 2021. **2**: p. 100116.
24. Turney, J.M., et al., *Psi4: an open-source ab initio electronic structure program.* Wiley Interdisciplinary Reviews: Computational Molecular Science, 2012. **2**(4): p. 556-565.
25. Garg, U., Y. Azim, and M. Alam, *In acid-aminopyrimidine continuum: experimental and computational studies of furan tetracarboxylate-2-aminopyrimidinium salt.* RSC advances, 2021. **11**(35): p. 21463-21474.
26. Bystrom, K. and B. Kozinsky, *CIDER: An expressive, nonlocal feature set for machine learning density functionals with exact constraints.* Journal of Chemical Theory and Computation, 2022. **18**(4): p. 2180-2192.
27. Lamichhane, A., *First-principles density functional theory studies on perovskite materials*. 2021, New Jersey Institute of Technology.
28. Gerolin, A. and M. Petrache, *Dispersion Interactions via Optimal Transport.*
29. Ramesh, G., et al., *Pyridinecarboxaldehydes: Structures, Vibrational Assignments and Molecular Characteristics Using Experimental and Theoretical Methods.* Brazilian Journal of Physics, 2023. **53**(2): p. 45.
30. Li, W., *Developing highly efficient electronic structure theory methods for large scale simulations*. 2021: University of California, Los Angeles.

31. Schmidt, J., et al., *Recent advances and applications of machine learning in solid-state materials science.* npj Computational Materials, 2019. **5**(1): p. 83.
32. Marques, M.A., et al., *octopus: a first-principles tool for excited electron–ion dynamics.* Computer Physics Communications, 2003. **151**(1): p. 60-78.
33. Grimme, S., C. Bannwarth, and P. Shushkov, *A robust and accurate tight-binding quantum chemical method for structures, vibrational frequencies, and noncovalent interactions of large molecular systems parametrized for all spd-block elements (Z= 1–86).* Journal of chemical theory and computation, 2017. **13**(5): p. 1989-2009.
34. Li, Y., *First principles calculations of the structure and electronic properties of pentacene based organic and zinc oxide based inorganic semiconducting materials*. 2012: University of North Texas.
35. Taer, E., et al. *Activated carbon electrode from banana-peel waste for supercapacitor applications*. in *AIP Conference Proceedings*. 2017. AIP Publishing.
36. Nguyen, T.N., P.A. Le, and V.B.T. Phung, *Facile green synthesis of carbon quantum dots and biomass-derived activated carbon from banana peels: synthesis and investigation.* Biomass Conversion and Biorefinery, 2020: p. 1-10.
37. Shuma, H., L. Mkayula, and Y. Makame, *Assessment of the effect of acid activation of kaolin from malangali on water defluoridation.* Tanzania Journal of Science, 2019. **45**(2): p. 279-296.
38. Ahmedzeki, N.S., S.M. Ali, and S.R. Al-Karkhi, *Synthesis and Characterization of Tri-Composite Activated Carbon.* Iraqi Journal of Chemical and Petroleum Engineering, 2017. **18**(3): p. 49-58.
39. Goldberg, S., *Equations and models describing adsorption processes in soils.* Chemical processes in soils, 2005. **8**: p. 489-517.
40. Johnson, A.I., et al., *The effect of self-interaction error on electrostatic dipoles calculated using density functional theory.* The Journal of chemical physics, 2019. **151**(17).
41. Cutini, M., L. Maschio, and P. Ugliengo, *Exfoliation energy of layered materials by DFT-D: Beware of dispersion!* Journal of Chemical Theory and Computation, 2020. **16**(8): p. 5244-5252.
42. Ashassi-Sorkhabi, H., et al., *Hybrid sol-gel coatings based on silanes-amino acids for corrosion protection of AZ91 magnesium alloy: Electrochemical and DFT insights.* Progress in Organic Coatings, 2019. **131**: p. 191-202.
43. Esrafili, M.D. and B. Nejadebrahimi, *Theoretical insights into hydrogenation of CO2 to formic acid over a single Co atom incorporated nitrogen-doped graphene: A DFT study.* Applied Surface Science, 2019. **475**: p. 363-371.
44. Lawal, O. and K. Adebowale, *Effect of acetylation and succinylation on solubility profile, water absorption capacity, oil absorption capacity and emulsifying properties of mucuna bean (Mucuna pruriens) protein concentrate.* Food/Nahrung, 2004. **48**(2): p. 129-136.
45. Brand, S.K., *I. Tin Silsesquioxanes as Analogs for the Open and Closed Sites in Tin-Containing Zeotype Beta and II. Enantiomerically Enriched, Polycrystalline Molecular Sieves*. 2017: California Institute of Technology.
46. Elhassan, M., et al., *Hydrochar from Shorea spp.: a dual-purpose approach for sustainable biofuel and efficient methylene blue adsorbent.* Biomass Conversion and Biorefinery, 2024: p. 1-15.
47. Veleva, S., et al., *Electrochemical Hybrid Supercapacitors Based on Activated Carbon and Iron Oxides.* Journal of Progressive Research in Chemistry, 2017.
48. Rani, B.J., et al., *Sn doped α-Fe2O3 (Sn= 0, 10, 20, 30 wt%) photoanodes for photoelectrochemical water splitting applications.* Renewable energy, 2019. **133**: p. 566-574.

49. He, X., et al., *FTIR and Raman spectroscopy characterization of functional groups in various rank coals.* Fuel, 2017. **206**: p. 555-563.
50. Soares, P.I., et al., *Thermal and magnetic properties of chitosan-iron oxide nanoparticles.* Carbohydrate polymers, 2016. **149**: p. 382-390.
51. Bakri, M.K.B. and E. Jayamani. *Comparative study of functional groups in natural fibers: Fourier transform infrared analysis (FTIR).* in *International Conference on Futuristic Trends in Engineering, Science, Humanities, and Technology (FTESHT-16).* 2016.
52. Kumar, D., et al., *Effect of precursor on the formation of different phases of iron oxide nanoparticles.* RSC Advances, 2015. **5**(10): p. 7138-7150.
53. Urian, Y., et al., *Study of the surface properties and particle-particle interactions in oleic acid-coated Fe3O4 nanoparticles.* Journal of Magnetism and Magnetic Materials, 2021. **525**: p. 167686.
54. Enders, A.A., et al., *Functional group identification for FTIR spectra using image-based machine learning models.* Analytical Chemistry, 2021. **93**(28): p. 9711-9718.
55. Jain, M., et al., *Development of iron oxide/activated carbon nanoparticle composite for the removal of Cr (VI), Cu (II) and Cd (II) ions from aqueous solution.* Water Resources and Industry, 2018. **20**: p. 54-74.
56. Kopac, T., K. Bozgeyik, and J. Yener, *Effect of pH and temperature on the adsorption of bovine serum albumin onto titanium dioxide.* Colloids and Surfaces A: Physicochemical and Engineering Aspects, 2008. **322**(1-3): p. 19-28.
57. Wong, S., et al., *Removal of acetaminophen by activated carbon synthesized from spent tea leaves: equilibrium, kinetics and thermodynamics studies.* Powder Technology, 2018. **338**: p. 878-886.
58. Akpomie, K.G. and J. Conradie, *Efficient adsorptive removal of paracetamol and thiazolyl blue from polluted water onto biosynthesized copper oxide nanoparticles.* Scientific Reports, 2023. **13**(1): p. 859.
59. Van Den Abeele, J., et al., *Gastrointestinal behavior of weakly acidic BCS class II drugs in man—case study of diclofenac potassium.* Journal of pharmaceutical sciences, 2016. **105**(2): p. 687-696.
60. Rainsford, K., *The discovery, development and novel actions of nimesulide*, in *Nimesulide—Actions and Uses*. 2005, Springer. p. 1-49.
61. Gharibzahedi, S.M. and S.M. Jafari, *7.1 Historical background of cyclodextrins.* Nanoencapsulation Technologies for the Food and Nutraceutical Industries, 2017: p. 187.
62. Kara, S., et al., *Modeling the effects of adsorbent dose and particle size on the adsorption of reactive textile dyes by fly ash.* Desalination, 2007. **212**(1-3): p. 282-293.
63. Hsieh, C.-T. and H. Teng, *Influence of mesopore volume and adsorbate size on adsorption capacities of activated carbons in aqueous solutions.* Carbon, 2000. **38**(6): p. 863-869.
64. Nandiyanto, A.B.D., et al., *Isotherm adsorption characteristics of carbon microparticles prepared from pineapple peel waste.* Communications in Science and Technology, 2020. **5**(1): p. 31-39.
65. Li, Z., et al., *Interpretation of the adsorption mechanism of Reactive Black 5 and Ponceau 4R dyes on chitosan/polyamide nanofibers via advanced statistical physics model.* Journal of Molecular Liquids, 2019. **285**: p. 165-170.
66. Rangabhashiyam, S., et al., *Relevance of isotherm models in biosorption of pollutants by agricultural byproducts.* Journal of Environmental Chemical Engineering, 2014. **2**(1): p. 398-414.

67. Al-Ghouti, M.A. and D.A. Da'ana, *Guidelines for the use and interpretation of adsorption isotherm models: A review.* Journal of hazardous materials, 2020. **393**: p. 122383.
68. Kundu, S. and A.K. Gupta, *Arsenic adsorption onto iron oxide-coated cement (IOCC): regression analysis of equilibrium data with several isotherm models and their optimization.* Chemical Engineering Journal, 2006. **122**(1-2): p. 93-106.
69. Yunusa, U. and M. Ibrahim, *Reclamation of malachite green-bearing wastewater using desert date seed shell: adsorption isotherms, desorption and reusability studies.* Chemsearch Journal, 2019. **10**(2): p. 112-122.
70. Mestre, A., et al., *Activated carbons for the adsorption of ibuprofen.* Carbon, 2007. **45**(10): p. 1979-1988.
71. Mansouri, H., et al., *Competitive adsorption of ibuprofen and amoxicillin mixtures from aqueous solution on activated carbons.* Journal of colloid and interface science, 2015. **449**: p. 252-260.
72. Önal, Y., C. Akmil-Başar, and Ç. Sarıcı-Özdemir, *Elucidation of the naproxen sodium adsorption onto activated carbon prepared from waste apricot: kinetic, equilibrium and thermodynamic characterization.* Journal of Hazardous Materials, 2007. **148**(3): p. 727-734.
73. Chen, Y.-G., et al., *Effect of contact time, pH, and ionic strength on Cd (II) adsorption from aqueous solution onto bentonite from Gaomiaozi, China.* Environmental Earth Sciences, 2011. **64**: p. 329-336.
74. Dimpe, K.M., *Preparation and characterization of carbon based adsorbents and their application for the removal of selected inorganic and organic pollutants*. 2018, University of Johannesburg (South Africa).
75. Kumar, J.A., et al., *One pot Green Synthesis of Nano magnesium oxide-carbon composite: Preparation, characterization and application towards anthracene adsorption.* Journal of Cleaner Production, 2019. **237**: p. 117691.
76. de Oliveira Sousa Neto, V., et al., *Evaluation of new chemically modified coconut shell adsorbents with tannic acid for Cu (II) removal from wastewater.* Journal of Applied Polymer Science, 2014. **131**(18).
77. Kowanga, K.D., et al., *Kinetic, sorption isotherms, pseudo-first-order model and pseudo-second-order model studies of Cu (II) and Pb (II) using defatted Moringa oleifera seed powder.* The journal of phytopharmacology, 2016. **5**(2): p. 71-78.
78. Konicki, W., et al., *Adsorption of cationic dyes onto Fe@ graphite core–shell magnetic nanocomposite: Equilibrium, kinetics and thermodynamics.* Chemical Engineering Research and Design, 2018. **129**: p. 259-270.
79. Ho, Y.-S. and G. McKay, *Pseudo-second order model for sorption processes.* Process biochemistry, 1999. **34**(5): p. 451-465.
80. Harrache, Z., et al., *Thermodynamic and kinetics studies on adsorption of Indigo Carmine from aqueous solution by activated carbon.* Microchemical Journal, 2019. **144**: p. 180-189.
81. Mariyam, A., et al., *Efficient batch and Fixed-Bed sequestration of a basic dye using a novel variant of ordered mesoporous carbon as adsorbent.* Arabian Journal of Chemistry, 2021. **14**(6): p. 103186.
82. Martins, R.J., R. Pardo, and R.A. Boaventura, *Cadmium (II) and zinc (II) adsorption by the aquatic moss Fontinalis antipyretica: effect of temperature, pH and water hardness.* Water Research, 2004. **38**(3): p. 693-699.
83. Baccar, R., et al., *Removal of pharmaceutical compounds by activated carbon prepared from agricultural by-product.* Chemical engineering journal, 2012. **211**: p. 310-317.
84. Clayton, J. and W. Giauque, *The heat capacity and entropy of carbon monoxide. Heat of vaporization. Vapor pressures of solid and liquid. Free energy to 5000 K. From spectroscopic data.* Journal of the American Chemical Society, 1932. **54**(7): p. 2610-2626.

85. Daikh, S., et al., *Equilibrium, kinetic and thermodynamic studies for evaluation of adsorption capacity of a new potential hybrid adsorbent based on polyaniline and chitosan for Acetaminophen.* Chemical Physics Letters, 2022. **798**: p. 139565.
86. Özcan, A., E.M. Öncü, and A.S. Özcan, *Kinetics, isotherm and thermodynamic studies of adsorption of Acid Blue 193 from aqueous solutions onto natural sepiolite.* Colloids and surfaces A: Physicochemical and engineering aspects, 2006. **277**(1-3): p. 90-97.
87. Dubey, S.P., et al., *Artemisia vulgaris-derived mesoporous honeycomb-shaped activated carbon for ibuprofen adsorption.* Chemical Engineering Journal, 2010. **165**(2): p. 537-544.
88. Mondal, S., et al., *Adsorption thermodynamics and kinetics of ranitidine hydrochloride onto superheated steam activated carbon derived from mung bean husk.* Journal of Environmental Chemical Engineering, 2015. **3**(1): p. 187-195.
89. Cazetta, A.L., et al., *Synthesis and application of N–S-doped mesoporous carbon obtained from nanocasting method using bone char as heteroatom precursor and template.* Chemical Engineering Journal, 2016. **300**: p. 54-63.
90. Jodeh, S., et al., *Adsorption of diclofenac from aqueous solution using Cyclamen persicum tubers based activated carbon (CTAC).* Journal of the Association of Arab Universities for Basic and Applied Sciences, 2016. **20**: p. 32-38.
91. Saadh, M., et al., *An enhanced adsorption of paracetamol drug using the iron-encapsulated boron carbide nanocage: DFT outlook.* Computational and Theoretical Chemistry, 2024. **1231**: p. 114421.
92. Bhuyan, A. and M. Ahmaruzzaman, *Recent advances in new generation nanocomposite materials for adsorption of pharmaceuticals from aqueous environment.* Environmental Science and Pollution Research, 2023. **30**(14): p. 39377-39417.
93. Olusegun, S.J., et al., *Iron-based materials for the adsorption and photocatalytic degradation of pharmaceutical drugs: a comprehensive review of the mechanism pathway.* Journal of Water Process Engineering, 2023. **51**: p. 103457.
94. Azizpourian, M., G. Kouchakzadeh, and Z. Derikvand, *Removal of pharmaceutical compounds from aqueous solution by clay-based synthesized adsorbents: adsorption kinetics and isotherms studies.* Chemical Papers, 2023. **77**(8): p. 4245-4264.
95. de Sá Costa, H.P., et al., *Adsorption of diclofenac and losartan using multi-walled carbon nanotubes functionalized with iron nanoparticles via the green route: Equilibrium, thermodynamics, and machine learning studies.* Journal of Water Process Engineering, 2024. **58**: p. 104923.
96. Castañeda Ramírez, A.A., et al., *Selective Adsorption of Aqueous Diclofenac Sodium, Naproxen Sodium, and Ibuprofen Using a Stable Fe3O4–FeBTC Metal–Organic Framework.* Materials, 2021. **14**(9): p. 2293.
97. Lv, Y., et al., *Efficient adsorption of diclofenac sodium in water by a novel functionalized cellulose aerogel.* Environmental Research, 2021. **194**: p. 110652.
98. Louis, H., et al., *Functionalized (–HCO,–OH,–NH2) Iridium-doped graphene (Ir@ Gp) nanomaterials for enhanced delivery of Piroxicam: Insights from quantum chemical calculations.* Journal of Molecular Liquids, 2023. **383**: p. 122068.

99. Binaymotlagh, R., et al., *Combined experimental and computational study of the in situ adsorption of piroxicam anions on the laser-generated gold nanoparticles.* The Journal of Physical Chemistry C, 2017. **121**(15): p. 8589-8600.

100. Musa, K.A., S. Omar, and L. Eriksson, *Mechanism of photoinduced photodegradation of piroxicam, the way to design new drugs of piroxicam derivatives.* Lebda Medical Journal, 2018. **4**(1): p. 154-167.